Intra-cavity absorption spectroscopy with narrow-ridge microfluidic quantum cascade lasers

Mikhail A. Belkin[1*], Marko Lončar[1], Benjamin G. Lee[1], Christian Pflügl[1], Ross Audet[1,2], Laurent Diehl[1], Federico Capasso[1*], David Bour[3,4], Scott Corzine[3,5] Gloria Höfler[3,6]

[1]*Harvard School of Engineering and Applied Sciences, Harvard University, Cambridge, MA 02138*
[2]*Current address: Department of Electrical Engineering, Stanford University, Stanford, CA 94350*
[3]*Agilent Laboratories, 3500 Deer Creek Road, Palo Alto, CA 94305*
[4]*Current address: Bridgelux, Sunnyvale, CA 94089*
[5]*Current address: Infinera, Sunnyvale, CA 94089*
[6]*Current address: Argos Tech, LLC, Santa Clara, CA 95051*
[*]*Corresponding authors: mbelkin@seas.harvard.edu, capasso@seas.harvard.edu*

Abstract: We demonstrate microfluidic laser intra-cavity absorption spectroscopy with mid-infrared λ≈9μm quantum cascade lasers. A deep-etched narrow ridge waveguide laser is placed in a microfluidic chamber. The evanescent tails of the laser mode penetrate into a liquid on both sides of the ridge. The absorption lines of the liquid modify the laser waveguide loss, resulting in significant changes in the laser emission spectrum and the threshold current. A volume of liquid as small as ~10pL may, in principle, be sufficient for sensing using the proposed technique. This method, similar to the related gas-phase technique, shows promise as a sensitive means of detecting chemicals in small volumes of solutions.

OCIS codes: (140.5960) Semiconductor lasers; (140.3070) Infrared and far-infrared lasers; (300.6260) Spectroscopy, diode lasers; (300.6340) Spectroscopy, infrared; (220.4000) Microstructure fabrication.

References and links

1. L. Diehl, D. Bour, S. Corzine, J. Zhu, G. Hofler, M. Loncar, M. Troccoli, and F. Capasso, "High-power quantum cascade lasers grown by low-pressure metal organic vapor-phase epitaxy operating in continuous wave above 400 K," Appl. Phys. Lett. **88**, 201115 (2006).
2. F. Capasso, C. Gmachl, D.L. Sivco, and A.Y. Cho, "Quantum cascade lasers," Physics Today **55**, 34-40 (2002).
3. D. Lin-Vien, N.B. Colthup, W.G. Fateley, and J.G. Grasselli, *The Handbook of Infrared and Raman Characteristic Frequencies of Organic Molecules* (Academic Press, Boston, MA 1991).
4. A. Kosterev and F. Tittel, "Chemical sensors based on quantum cascade lasers," IEEE J. Quantum Electron. **38**, 582-591 (2002).
5. C. Charlton, F. de Melas, A. Inberg, N. Croitoru, and B. Mizaikoff, "Hollow-waveguide gas sensing with room-temperature quantum cascade lasers, " IEE Proc. Optoelectron. **150**, 306-309 (2003)
6. B. Lendl, J. Frank, R. Schindler, A. Müller, M. Beck, and J. Faist, "Mid-infrared quantum cascade lasers for flow injection analysis," Anal. Chem. **72**, 1645 (2000).
7. J. Chen, Z. Liu, C. Gmachl, D. Sivco, "Silver halide fiber-based evanescent-wave liquid droplet sensing with room temperature mid-infrared quantum cascade lasers, ", Opt. Express **13**, 5953-5960 (2005), http://www.opticsinfobase.org/abstract.cfm?URI=oe-13-16-5953.
8. C. Charlton, A. Katzir, and B. Mizaikoff, "Infrared evanescent field sensing with quantum cascade lasers and planar silver halide waveguides," Anal. Chem. **77**, 4398-4403 (2005).
9. C. Charlton, M. Giovannini, J. Faist, B. Mizaikoff, "Fabrication and characterization of molecular beam epitaxy grown thin-film GaAs waveguides for mid-infrared evanescent field chemical sensing," Anal. Chem. **78**, 4224-4227 (2006).
10. S. Schaden, A. Domínguez-Vidal, and B. Lendl, "Quantum cascade laser modulation for correction of matrix-induced background changes in aqueous samples," Appl. Phys. B **86**, 347-351 (2007).

#84247 - $15.00 USD Received 18 Jun 2007; revised 12 Aug 2007; accepted 16 Aug 2007; published 21 Aug 2007

11. V.M. Baev, T. Latz, and P.E. Toschek, "Laser intracavity absorption spectroscopy," Appl. Phys. B **69**, 171-202 (1999).
12. D. Erickson and D. Li, "Integrated microfluidic devices," Anal. Chim. Acta **507**, 11-26 (2004).
13. D. Psaltis, S.R. Quake, and C. Yang, "Developing optofluidic technology through the fusion of microfluidics and optics," Nature **442**, 381-386 (2006).
14. C. Monat, P. Domachuk, and B.J. Eggleton, "Integrated optofluidics: a new river of light," Nature Photon. **1,** 106-114 (2007).
15. E. Verpoorte, "Chip vision – optics for microchips," Lab Chip **3**, 42N-52N (2003).
16. L. Diehl, B.G. Lee, P. Behroozi, M. Lončar, M.A. Belkin, F. Capasso, T. Aellen, D. Hofstetter, M. Beck, and J. Faist, "Microfluidic tuning of distributed feedback quantum cascade lasers," Opt. Express **14,** 11660-11667 (2006), http://www.opticsinfobase.org/abstract.cfm?URI=oe-14-24-11660.
17. E. Verpoorte, A. Manz, H. Lüdi, A.E. Bruno, F. Maystre, B. Krattiger, H. M. Widmer, B.H. van der Schoot, and N.F. de Rooij, "A silicon flow cell for optical detection in miniaturized total chemical analysis systems," Sens. Actuators B **6**, 66-70 (1992).
18. K.B. Mogensen, N.J. Petersen, J. Hübner, and J.P. Kutter, "Monolithic integration of optical waveguides for absorbance detection in microfabricated electrophoresis devices," Electrophoresis **22**, 3930–3938 (2001).
19. J. C. Galas, C. Peroz, Q. Kou, and Y. Chen, "Microfluidic dye laser intracavity absorption," Appl. Phys. Lett **89**, 224101 (2006).
20. J. Faist, M. Beck, T. Aellen, and E. Gini, "Quantum-cascade lasers based on bound-to-continuum transition," Appl. Phys. Lett. **78,** 147-149 (2001).
21. R. Maulini, M. Beck, J. Faist, and E. Gini, "Broadband tuning of external cavity bound-to-continuum quantum-cascade lasers," Appl. Phys. Lett. **84,** 1659-1661 (2004).
22. M. Lončar, B.G. Lee, L. Diehl, M. Belkin, F. Capasso, M. Giovannini, J. Faist, and E. Gini, "Design and fabrication of photonic crystal quantum cascade lasers for optofluidics," Opt. Express **15,** 4499-4514 (2007), http://www.opticsinfobase.org/abstract.cfm?URI=oe-15-8-4499.
23. M. Beck, D. Hofstetter, T. Aellen, J. Faist, U. Oesterle, M. Ilegems, E. Gini, H. Melchior "Continuous wave operation of a mid-infrared semiconductor laser at room temperature," Science **295,** 301-305 (2002).
24. J.Z. Chen, Z. Liu, Y.S. Rumala, D.L. Sivco, and C.F. Gmachl, "Direct liquid cooling of room-temperature operated quantum cascade lasers," Electron. Lett. **42,** 534-535 (2006).

1. Introduction

Mid-infrared (mid-IR) quantum cascade lasers (QCLs) have recently become a mature technology providing continuous-wave operation with hundreds of milliwatts of output power at and above room temperature [1]. The emission wavelength of these devices can be adjusted by changing the width of semiconductor quantum wells and spans continuously from 3.4 to 24 μm [2], covering the entire mid-IR fingerprint region [3]. This allows one to use QCLs for a variety of chemical sensing applications, including gas [4,5] and liquid [6-10] sensing. In this work we report a microfluidic sensor for detecting chemicals in small volumes of solutions based on laser intra-cavity absorption spectroscopy (ICAS) using a $\lambda \approx 9$ μm QCL.

Since the mid-1970s, laser ICAS has been used as a highly sensitive spectroscopic technique [11]. In this method, the analyte is placed within the laser cavity. The absorption lines of the analyte modify the laser losses, causing significant changes in the laser threshold and emission spectrum. Because of the strong competition between different laser modes, very weak absorption features of the sample can imprint signatures in the laser emission spectrum. Alternatively, high sensitivity can also be achieved in laser ICAS by employing the nonlinear nature of the lasing process when the laser is operated close to its threshold. In this case, small changes in the laser loss may result in large changes in the laser emission intensity. We note that the latter method is typically less sensitive than the former. Traditionally, ICAS has been applied to gases. Liquids typically have strong absorption features that preclude the need for a long absorption path length. Additionally, the absorption lines of liquids are typically very broad, while for sensitive ICAS, the linewidths of the absorption lines of the analyte must be much smaller than the laser gain bandwidth [11].

Microfluidics is a growing field with important applications in biotechnology, chemical synthesis, and medicine [12-16]. Microfluidic devices offer the ability to work with smaller reagent volumes, shorter reaction times, and the possibility of parallel operation. The small

#84247 - $15.00 USD Received 18 Jun 2007; revised 12 Aug 2007; accepted 16 Aug 2007; published 21 Aug 2007

volume of analyte in microfluidic systems makes it difficult to use conventional absorption measurements for analysis because of the limited optical path length [15]. Several solutions have been suggested, including multi-path cells [17] and z-shaped cells [18]. Microfluidic ICAS may provide a more sensitive and compact solution. Recently, microfluidic ICAS has been demonstrated in the visible spectral region using an optically pumped microfluidic dye laser [19]. The mid-IR fingerprint region is, however, far more broadly used for chemical sensing and QCLs are excellent injection pumped sources in this region. Quantum cascade lasers can be designed with a very large homogeneously broadened gain bandwidth, with full width at half maximum (FWHM) of ~300cm^{-1} [20,21]. This is significantly larger than a typical FWHM of the absorption lines of liquids in mid-IR (~20 cm^{-1}) and may make sensitive microfluidic ICAS possible [11].

2. Fabrication and experimental results

Our microfluidic QCL ICAS sensor is based on a deep-etched narrow-ridge QCL with the ridge walls exposed to a liquid. For a sufficiently small ridge width, the evanescent tails of the laser mode have significant overlap with the liquid on both sides of the ridge (Fig. 1(a)). The liquid absorption lines modify the modal loss and cause a change in the QCL threshold current and emission spectrum. In Fig. 1(b) we plot the dependence of the laser mode loss on the liquid absorbance and specify the modal overlap with the liquid for a TM_{00} mode in a λ=9 μm QCL with a standard dielectric waveguide structure (described below) and different ridge widths. The modal overlap with the liquid increases as the ridge becomes narrower, resulting in a strong dependence of the laser modal loss on the liquid absorption for very narrow ridges. For a QCL with a 2-μm-wide ridge, the laser modal losses increase from intrinsic values of 5-10 cm^{-1} to more than 100 cm^{-1} as the imaginary part of the liquid refractive index grows from *0* to *0.2i*, the latter being a typical number for strong mid-IR absorption lines in liquids. Thus, we expect to see dramatic changes in the laser threshold current and emission spectrum for narrow-ridge QCLs as they become submerged in an absorbing liquid. A very small volume of liquid is required for sensing in these devices. The penetration depth of the evanescent tails of the laser mode intensity on both sides of the ridge is calculated to be between 250 and 300 nm for ridge widths between 6 μm and 2 μm, respectively. For a typical ICAS QCL with a 2.5-mm-long, 2 to 6-μm-wide, and 10-μm-high ridge we thus estimate the required liquid volume to be ~10 picoliters, providing appropriate microfluidic chamber material and delivery

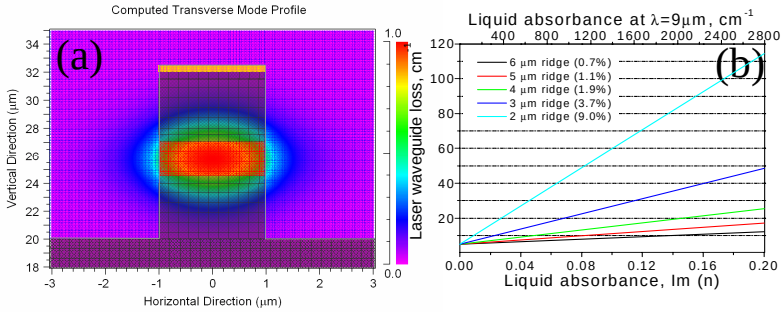

Fig. 1. (a) Simulated electric field distribution for a TM_{00} mode in a deep-etched 2-μm-wide ridge quantum cascade laser with a gold electrical contact on top, surrounded by a liquid. The laser active region is shown in red. (b) Dependence of the TM_{00} laser mode losses on liquid absorbance for deep-etched ridge waveguide quantum cascade lasers with various ridge widths. Also listed is the percentage of modal overlap with the liquid (in intensity) for ridges of various widths. Liquid refractive index, Re(n), is assumed to be 1.3 in the simulations. Simulations were performed using commercial software packages, BeamPROP (R-Soft Design Group, Inc) and COMSOL Multiphysics (COMSOL, Inc).

#84247 - $15.00 USD Received 18 Jun 2007; revised 12 Aug 2007; accepted 16 Aug 2007; published 21 Aug 2007

system. Note that we have chosen to produce narrow-ridge QCLs for ICAS using evanescent fields instead of introducing analyte directly into a laser cavity, because the latter would require chamber walls with very good antireflection coatings or photonic crystal laser structures [22], which are more difficult to fabricate.

We fabricated narrow-ridge QCLs using QCL material grown by metal organic vapor-phase epitaxy. The laser active region is based on a bound-to-continuum design described in Ref. [21]. The laser waveguide core consists of a 2.4-μm-thick active region, composed of 35 stages, sandwiched between two 0.58-μm-thick $In_{0.53}Ga_{0.47}As$ layers Si-doped to 3×10^{16} cm^{-3}. The top waveguide cladding is provided by 4 μm-thick layer of InP Si-doped to 1×10^{17} cm^{-3} and a 0.5-μm-thick layer of InP Si-doped to 5×10^{18} cm^{-3}. The lower waveguide cladding is provided by 4 μm of InP Si-doped to 1×10^{17} cm^{-3}, grown on top of the InP substrate, which is n-doped to 3×10^{18} cm^{-3}. The devices are processed into deep-etched ridge waveguides with ridge widths of 3, 4, 5, and 6 μm. A 1.2-μm-thick layer of gold is deposited on top of the upper waveguide cladding by electron-beam evaporation. We then define the ridges using Microposit SU-8 2005 photoresist mask and a combination of argon-milling and inductively coupled plasma reactive ion etching to etch trough the 1.2-μm-thick layer of gold and all the layers of the QCL structure down to the InP substrate. In order to keep the side walls of the ridges exposed to the liquid, the gold layer on top of the laser ridge is connected to the bonding pad by the layer of gold on the surface of one of the ridge facets, see Fig. 2(a). This facet has a distinct T-shape and is defined along with the rest of the ridge by inductively coupled plasma reactive ion etching, using the same SU-8 2005 mask. The sidewall of the facet is insulated with a 300 nm-thick Si_3N_4 layer deposited via chemical vapor deposition. The gold stripe runs from the bonding pad at the bottom of the facet to the gold layer on top of the ridge, providing both a high reflection coating and an electrical contact, Fig. 2(a). The other facet of the laser is defined by cleaving the wafer. Scanning electron microscope images of the processed devices are shown in Fig. 2(b,c). We note that the devices in Fig. 2(b,c) have significant surface roughness, which originates in the argon-milling step (see above). We hope to reduce the surface roughness in future processing runs, using Si_3N_4 as a mask and/or employing other device geometries.

In order to reliably deliver liquids to the QCL ICAS sensors, the devices were encapsulated into poly-dimethyl-siloxane (PDMS) chambers with a silicon window positioned

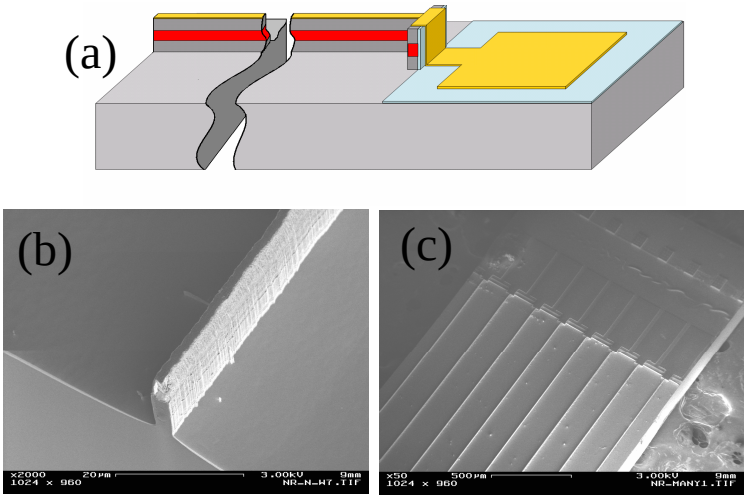

Fig. 2. (a) Schematics of a narrow-ridge quantum cascade laser for inracavity absorption spectroscopy. (b,c) Scanning electron microscope images of the processed devices: (b) the cleaved edge of a laser ridge and (c) several narrow-ridge quantum cascade lasers processed on the same substrate.

#84247 - $15.00 USD Received 18 Jun 2007; revised 12 Aug 2007; accepted 16 Aug 2007; published 21 Aug 2007

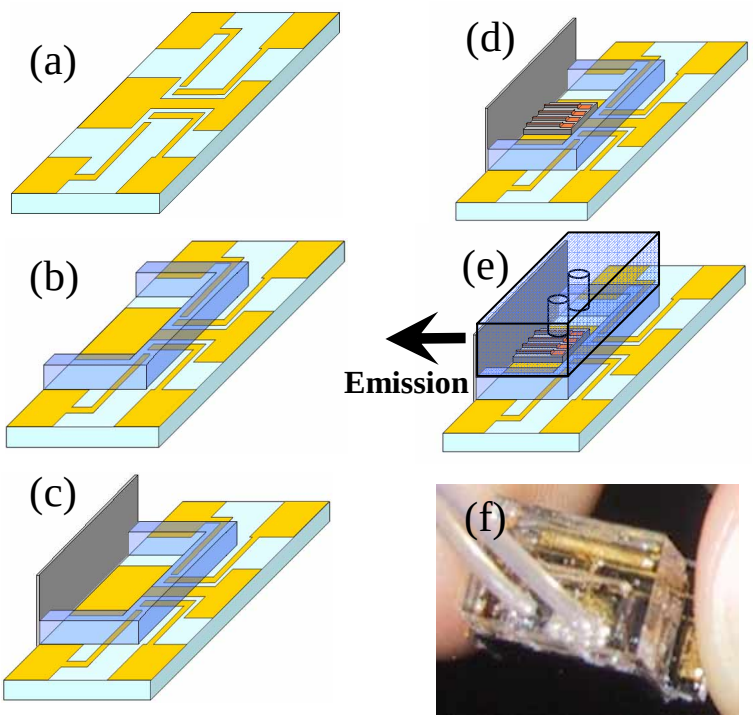

Fig. 3. (a)-(d) Different steps in fabrication of a microfluidic chamber; (e) devices after encapsulation; (f) a photograph of encapsulated devices.

in front of the cleaved laser facet for optical detection of the laser output. The encapsulation procedure is illustrated in Fig. 3. First, we prepare 8×17 mm glass slides with 300-nm-thick gold contacts deposited by thermal evaporation, Fig. 3(a). Then, a three-wall PDMS chamber with 3-mm-high and 3-mm-thick walls is placed on top of the glass slide; a thin layer of uncured PDMS is used for adhesion, Fig. 3(b). The structure is then baked for 8 hours at 70°C. Next, a 8-mm-wide, 5-mm-high silicon window is cleaved from a 350-μm-thick semi-insulating double-side-polished silicon wafer and attached to the camber opening, Fig. 3(c). Again, uncured PDMS is used for adhesion and the structure is baked. The cleaved lasers are then placed in the chamber such that the cleaved facets are within 20 μm of the silicon window. The lasers are soldered to the top of the central gold contact on the glass slide using Indium solder, Fig. 3(d). We then wire bond the lasers to the side contacts on the glass slide. Finally, a 5-mm-thick PDMS cap with microfluidic inlet and outlet tubing is placed on top and the chamber is sealed using small quantities of uncured PDMS and baking, Fig. 3(e). The resulting chambers have inner dimensions of 4 mm by 6 mm by 2 mm, corresponding to a volume of ~50 μL, and are very robust and allow for easy delivery of various liquids to the lasers. The final device is approximately 17 mm long, 8 mm wide and 8 mm tall, see Fig. 3(f).

After the encapsulation, the lasers were tested in pulsed mode at room temperature with 20 ns pulses at a repetition rate of 80 kHz. Devices with ridge widths of 5 and 6 μm operated reliably at room temperature. The maximum operating temperature of QCLs with 4-μm-wide ridges was approximately 290K; 3-μm-wide-ridge QCLs operated only at cryogenic temperatures. We attribute the deterioration of the narrow-ridge QCL performance with decreasing ridge width to the ridge wall roughness (see Fig. 2(b)) that induces significant scattering losses. In Fig. 4(a) we plot light output versus current and current versus voltage characteristics of a typical device with a 5-μm-wide, 2.5-mm-long ridge, with and without various liquids in the PDMS chamber. Note that the shape of the current-voltage curve is influenced by the ohmic resistance in the gold contacts on the glass slide and in the gold

#84247 - $15.00 USD Received 18 Jun 2007; revised 12 Aug 2007; accepted 16 Aug 2007; published 21 Aug 2007

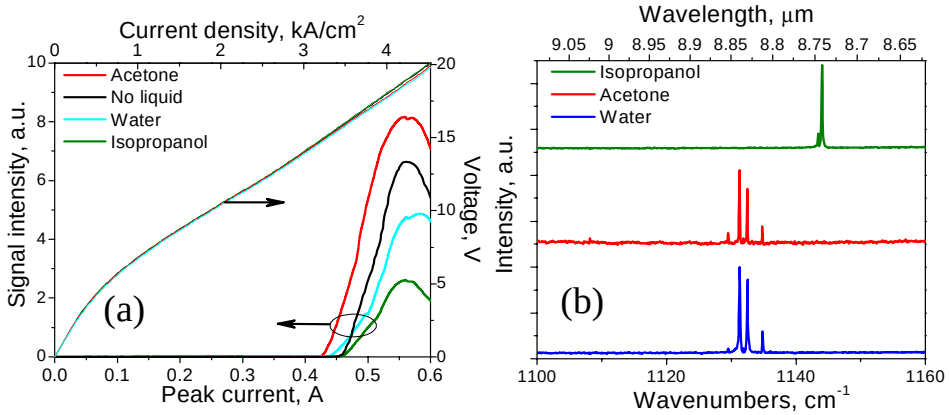

Fig. 4. (a) Current versus voltage (right axis) and light output versus current (left axis) characteristics obtained at 297K in pulsed mode (20ns pulses at 80kHz) with a 5-μm-wide 2.5-mm-long ridge encapsulated device with and without liquids. The threshold currents are ≈424±1.5 mA for device immersed in acetone, ≈435±1.5 mA for a devices immersed in water, ≈458±1.5 mA for a device immersed in isopropanol, and ≈457±1.5 mA for a device without liquids. (b) Emission spectra of the same device immersed in various liquids.

contact on top of the laser ridge. The current-voltage characteristics in Fig. 4(a) also show that there is no significant leakage current as the laser ridge is immersed in the liquids. The laser emission spectra near threshold are shown in Fig. 4(b). The spectra were taken with a Fourier transform infrared spectrometer (FTIR) equipped with a nitrogen-cooled mercury cadmium telluride (MCT) detector. The emission spectra for a device submerged in water and acetone are similar to those taken without liquid, while the emission spectrum for a device submerged in isopropanol is very different, with the emission lines clearly shifted from approximately 1130-1135 cm^{-1} to approximately 1144 cm^{-1}. This behavior can be explained by studying the absorption spectra of the liquids, shown in Fig. 5(a). While both water and acetone have no absorption features near the laser gain peak, situated at approximately 1130-1135 cm^{-1}, isopropanol has a strong absorption line there. As a result, the emission frequency of a device submerged in isopropanol shifts to 1144 cm^{-1}, a position of minimal absorption, see Fig. 5(a).

The threshold current density for devices with 5-μm-wide, 2.5-mm-long ridges, without liquids, is approximately 3.5 kA/cm^2, significantly larger than the threshold current density of

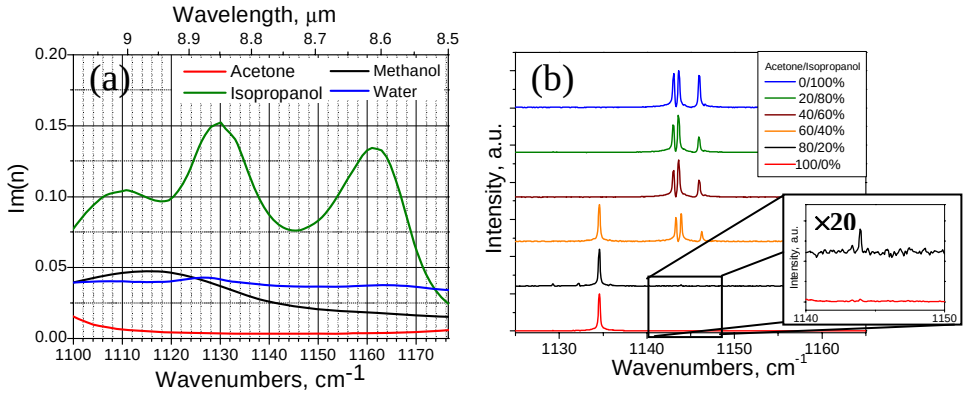

Fig. 5. (a) Absorption spectra of liquids used in the experiments. (b) Emission spectra of an encapsulated 5-μm-wide, 2.5-mm-long ridge device immersed in various mixtures of isopropanol and acetone.

#84247 - $15.00 USD Received 18 Jun 2007; revised 12 Aug 2007; accepted 16 Aug 2007; published 21 Aug 2007

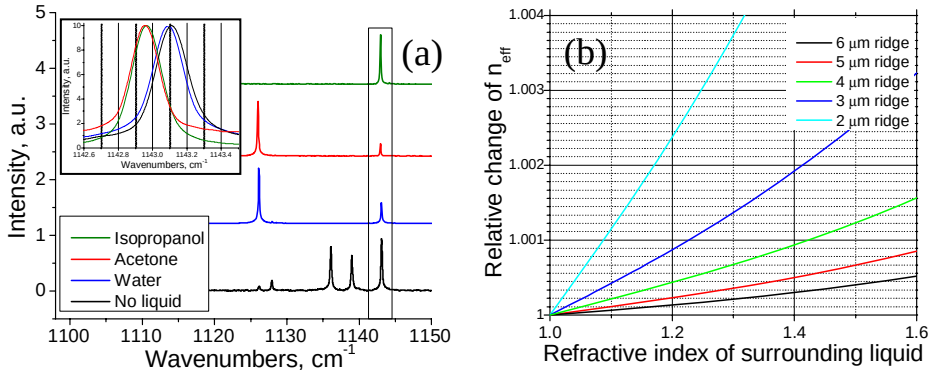

Fig. 6. (a) Emission spectra of a 5-μm-wide 2.5-mm-long ridge encapsulated device with and without liquids. The spectra were obtained at 297 K. The device was driven with 540 mA current pulses, 20-ns-long at the repetition rate of 80 kHz. Note that the data in Figs. 4 and 6 is obtained with a different device. Inset shows the zoom-in of the laser modes situated around 1143 cm^{-1} (b) Dependence of the TM_{00} laser mode effective refractive index on a liquid refractive index for deep-etched ridge waveguide quantum cascade lasers with various ridge widths. The liquid absorbance, In(n), is assumed to be 0 in the simulations. Simulations were performed using commercial software packages, BeamPROP (R-Soft Design Group, Inc). Note that the dependence of the effective refractive index of the laser mode on the liquid refractive index may be used for microfluidic tuning of quantum cascade lasers [16].

2.5 kA/cm^2 measured for traditional 18-μm-wide ridge lasers processed from the same material. Interestingly, the threshold current for our devices is significantly lower when the ridges are immersed in acetone than when the laser ridge is kept dry, despite the fact that acetone, having a refractive index of ~1.35, reduces slightly the reflection feedback from the cleaved facet of the device. We believe that this is an indication that the ridge surface roughness does cause significant loss in our devices. Acetone decreases the refractive index contrast at the ridge surface and reduces the scattering from the ridge surface roughness. Other liquids (which have similar refractive indices to that of acetone) have similar effect, but the threshold current reduction for acetone is the strongest as acetone has virtually no absorption at the laser emission frequency.

We have ruled out as another possible reason for the lower threshold current acetone evaporation and the attendant reduction of the laser ridge temperature. To do that, we have compared the emission spectra of the encapsulated 5-μm-wide, 2.5-mm-long ridge device with and without liquids. The spectra are shown in Fig. 6(a). The change in the laser ridge temperature causes the change of the refractive index of the laser waveguide, which results in the frequency shift of the laser Fabry-Perot modes following a well-known [23] coefficient of ≈-0.075 cm^{-1} per degree K, which we have verified it in our lasers by varying the substrate temperature. Thus, the "liquid cooling" effect should show up as a blue-shift of the laser modes when the liquid is added. Comparing the laser emission spectra with and without liquids, shown in the inset in Fig. 6(a), we see that the frequencies of the laser modes are red-shifted by ≈0.02 cm^{-1}, ≈0.14 cm^{-1}, and ≈0.15 cm^{-1} for water, isopropanol, and acetone, respectively. The red-shift appears, because the laser mode is partly outside of the laser ridge and the refractive index of the liquid modifies the effective refractive index of the laser mode. From the data in Fig. 6(b), we can estimate that, for a 5-μm-wide laser ridge, the addition of a liquid with the refractive index of 1.35 red-shifts the laser mode by ~0.4 cm^{-1} in comparison the laser emission without liquids. The difference of this number and the observed spectral red-shift of the laser modes may be due to the refractive index dispersion of the liquids in the mid-infrared or due to the "liquid cooling" effect. It is clear, however, that the "liquid cooling" effect of acetone cannot account for more than ~0.25 cm^{-1} of the spectral shift, which

#84247 - $15.00 USD Received 18 Jun 2007; revised 12 Aug 2007; accepted 16 Aug 2007; published 21 Aug 2007

would correspond to ~3.3° K ridge temperature change. We further note that, similarly, the difference between the ridge temperatures of a device immersed in acetone, isopropanol, and water is within 2°.

We have checked, by varying the substrate temperature for the same device in the range 280-310° K, that the laser threshold current changes by approximately 1.8 mA per 1° K of the temperature increase. Thus, the "acetone cooling" effect may account for no more than ~6 mA of the observed threshold current change of ~33mA, reported in Fig. 4(a), when the laser ridge is immersed in acetone. The reason for a small liquid cooling effect in our devices, in comparison with that observed in Ref. [24] is that the PDMS chamber is fully sealed and the lasers are operated with very short (20 ns at 80 kHz repetition rate) current pulses. We note that even shorter (<10ns) current pulses can be used to further reduce laser ridge heating.

For chemical detection, laser ICAS techniques utilize either laser emission spectrum changes or laser threshold changes due to analyte absorption. Below, we investigate both approaches with our QCL ICAS microfluidic sensors, using different mixtures of isopropanol and acetone. We refer the reader to Ref. [11] for a detailed theoretical description of these approaches.

In Fig. 5(b) we show the emission spectra of 5-μm-wide, 2.5-mm-long ridge device submerged in different mixtures of isopropanol and acetone. The spectra were taken at pump currents close to the peak of the light output, using 20 ns pulses at a repetition rate of 80 kHz. The laser emission frequency shifts from the peak of the laser gain position at approximately 1134 cm^{-1} to the minimum of isopropanol absorption position at 1143-1146 cm^{-1} as the fraction of isopropanol in the solution rises. The peaks at 1143-1146 cm^{-1} appear in the laser emission spectrum at isopropanol concentration level of approximately 20% in the isopropanol/acetone solution, see Fig. 5(b).

We note that the laser emission spectra, shown in Figs. 4(b), 5(b), and 6(a), do not display a series of equally spaced Fabry-Perot modes with the frequency spacing of ~0.65 cm^{-1} expected for a 2.5-mm-long QCL. We believe that this is caused by the ridge roughness that provides feedback to some of the laser modes and influences the lasing mode selection. In laser ICAS, the sensitivity of the laser emission spectrum to the analyte absorption arises from the mode competition [11]. In future work, we expect to fabricate devices with reduced surface roughness, which should result in their higher spectral sensitivity to analyte absorption.

In the other approach for chemical detection using microfluidic QCL ICAS, we set the pump current slightly above threshold for a device submerged in acetone and detect the laser

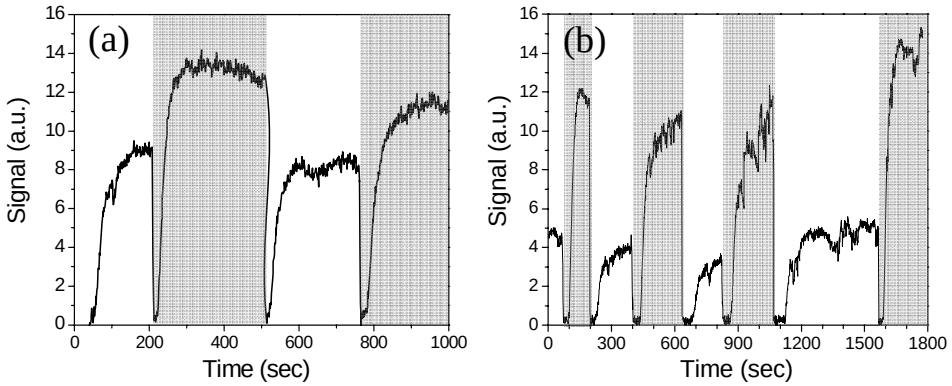

Fig. 7. Emission power from a 5-μm-wide 2.5-mm-long ridge encapsulated device immersed in (a) acetone (shaded areas) and a 1% volume solution of isopropanol in acetone (clear areas) and (b) methanol (shaded areas) and 5% volume solution of isopropanol in methanol (clear areas). The laser was operated in pulsed mode with 9 ns pulses at 80 kHz repetition rate. The peak current was kept fixed slightly above the lasing threshold.

#84247 - $15.00 USD Received 18 Jun 2007; revised 12 Aug 2007; accepted 16 Aug 2007; published 21 Aug 2007

peak output power change for a 1% volume solution of isopropanol in acetone. Here we utilize the fact that the laser emission power near threshold is very sensitive to the amount of pump current in excess of the threshold value [11]. Because the threshold current in quantum cascade lasers is sensitive to the device temperature, the encapsulated devices are mounted on a temperature-stabilized heatsink to keep their temperature constant at 15°C +/- 0.1°. We sequentially fill the device chamber with acetone and a 1% volume solution of isopropanol in acetone and observe changes in the emission power, Fig. 7(a). The liquids are kept at room temperature of ~25°C; therefore, as fresh liquid is injected into the chamber, the laser heats up to ~25°C and shuts off because the threshold current at 25°C is larger than that at 15°C. As the temperature of the device and liquid becomes that of the heatsink, the laser power recovers and stabilizes, Fig. 7(a). Because of isopropanol absorption, the threshold current for a device submerged in a 1% isopropanol solution in acetone is higher than that for a device submerged in acetone only, resulting in lower laser output power at a fixed current. In Fig. 7(b) we plot similar data for the solutions of isopropanol in methanol. Here both liquids have significant absorption at the laser emission frequency, see Fig. 5(a), however isopropanol absorption is approximately three times stronger than that of methanol. The laser pump current is set slightly above threshold for a device submerged in methanol. Thus, the laser gain compensates methanol absorption at the laser emission frequency. As the methanol is substituted with 5% isopropanol solution in methanol and the temperature of the device stabilizes, the new laser power level is significantly lower due to the threshold current change from additional isopropanol absorption, Fig. 7(b). In such a way, our devices can be utilized to detect absorbing analytes in solvents that themselves have absorption at the probe wavelength. This may be valuable for probing chemical and biological analytes in water in the mid-IR, since water has strong absorption over the entire mid-IR spectral range, see, e.g., Fig. 5(a), and traditional mid-IR absorption spectroscopy of water solutions is difficult to perform.

The sensitivity of ICAS is described using the effective absorption length, L_{eff}, defined as the cell pathlength required to obtain the equivalent signal change due to analyte absorption in traditional absorption spectroscopy [11],

$$L_{eff} = -\frac{\ln(I/I_0)}{\alpha}, \quad (1)$$

where I_0 is the ICAS signal without analyte, I is the signal with analyte, and $\alpha=4\pi Im(n)/\lambda$ is the absorbance of the analyte, n being the refractive index. For the data presented in Fig. 7(a), we estimate $I/I_0 \approx 0.75$ and obtain $L_{eff} \approx 170$ μm. For the data presented in Fig. 7(b), we estimate $I/I_0 \approx 0.35$ and obtain $L_{eff} \approx 165$ μm. These values are many orders of magnitude smaller than those obtained in ICAS experiments with gases, where kilometer-scale values are routinely obtained [11]. However, the sensitivity limit in our devices is currently determined by the laser power fluctuations due to temperature or laser power supply fluctuations, rather than spontaneous emission noise [11], leaving significant room for sensitivity improvement.

Several steps can be implemented in order to improve L_{eff} in our sensors. The results presented here have been obtained with 5-μm-wide ridge devices. From Fig. 1(b) we see that the modal overlap with liquid grows significantly for narrower ridges. The modal overlap and the sensitivity to liquid absorption are expected to increase ~9 times for 2-μm-wide ridges in comparison with 5-μm-wide ridges. Currently, the losses due to the walls' roughness limit the performance of the devices with ridge width below 5 μm to temperatures lower than room temperature. We expect to be able to significantly reduce the wall roughness in future processing runs. With narrower ridges, improved processing, better temperature control, and a more stable power supply, we expect to increase L_{eff} by at least two orders of magnitude.

3. Conclusion

In conclusion, we have experimentally demonstrated microfluidic mid-IR injection-pumped ICAS sensors based on deep-etched narrow-ridge λ≈9 μm QCLs. Our devices have demonstrated sensitivity equivalent to a 170-μm-thick absorption cell, while a volume of

#84247 - $15.00 USD Received 18 Jun 2007; revised 12 Aug 2007; accepted 16 Aug 2007; published 21 Aug 2007

liquid as small as ~10pL is, in principle, sufficient for sensing, providing appropriate chamber material and delivery system. In future work, we expect to increase the sensitivity of our devices several-fold.

The chemicals used in our experiments were selected for the purpose of demonstration of the proposed technique. After establishing the sensitivity of the proposed method, our devices may be used for a variety of relevant chemical sensing problems [6-10]. We note that the sensitivity of the proposed method depends only on the absorption coefficient of the analyte at laser emission frequency. The QCL active region can be specifically designed to target absorption lines of any chemical compound of interest in the mid-infrared chemical "fingerprint" region. We believe that our devices may become useful for a variety of mid-IR sensing applications in microfluidic systems.

Acknowledgments

This work was supported by the DARPA Optofluidic Center under grant HR0011-04-1-0032. The structures were processed in the Center for Nanoscale Systems (CNS) at Harvard University. Harvard-CNS is a member of the National Nanotechnology Infrastructure Network. We would like to acknowledge Yuan Lu, Jonathan Fan, and Mariano Troccoli for their assistance.

#84247 - $15.00 USD Received 18 Jun 2007; revised 12 Aug 2007; accepted 16 Aug 2007; published 21 Aug 2007